

# *Ab initio* investigation of the groundstate, magnetic, electronic, and optical properties of polyynes and cumulene prototypes

Carlo Motta, Marco Cazzaniga, Andrea Bordoni, and Katalin Gaál-Nagy\*

*Università degli Studi di Milano, Dipartimento di Fisica,  
CNISM-CNR-INFM, via Celoria 16, I-20133 Milano, Italy*

(Dated: February 3, 2022)

We have investigated polyynes and cumulene prototypes based on the density-functional theory. Our independent-particle spectra show that the various carbynes can be distinguished by optical properties comparing the low-energy spectral structure as well as using very general considerations. The latter conclusion is supported by results based on the random-phase approximation including local-field effects.

PACS numbers: 31.15.A- 31.15.es 78.67.-n 31.15.ap

## I. INTRODUCTION

Carbon-based materials possess many potential ability for future technologies.<sup>1,2,3</sup> Carbon atoms (C) are known to have three bonding states resulting from hybridization of the atomic orbitals:  $sp^3$  (diamond),  $sp^2$  (graphite and fullerenes), and  $sp$ . While the importance of  $sp^2$  structure is by now confirmed, a lot of interest is growing around  $sp$  carbon allotropes, named carbynes.

The formation of  $sp$  carbon chains is expected in the initial stage of small carbon cluster formation, on the road towards the fullerene structure, when the  $sp^2$  phase is energetically less favorable.<sup>4</sup> Furthermore, the interpretation of some IR bands from the interstellar dust could be related to the presence of  $sp$ -coordinated carbon.<sup>5</sup> Carbon chains are also interesting systems because they can be found connecting different graphene fragments.<sup>6,7</sup> Experimental work has been recently devoted to the production and investigation of  $sp$ -hybridized carbon structures.<sup>4,7,8,9,10,11</sup> Furthermore, pure-carbon solid containing carbynoid structures have been produced by cluster beam deposition in the last years.<sup>8</sup> Carbynes survive landing because they are stabilized and protected by the  $sp^2$  network.

Open carbon (C) chains of any length must be terminated by molecular complexes to ensure stability, of course. In principle, linear carbon chains can be obtained with two different terminations:  $sp^3$  termination, resulting in carbon atoms linked by alternated single and triple bonds (polyynes) and so with alternating bond length, and  $sp^2$  termination, resulting in double bonds (cumulene).<sup>12</sup> Experimentally polyynes are found to be more stable than cumulenes.<sup>5</sup> In this work, we have chosen hydrogen (H) terminations. The choice of saturating the chains with one or two hydrogen atoms reflects the experimental fact, that the carbynes attached to graphene fragments can be bound with a variable number of carbon atoms. Optical spectra of carbyne are related to the typical  $\pi$ -bonds of carbon valence electrons, which are degenerate only in the polyyne case. Electronic spectra have been measured before for different polyyne molecules in neon matrices<sup>13</sup> or in gas phase.<sup>14</sup>

The present article reports on the *ab initio* study of the optical properties of cumulene and polyyne prototypes, within the density-functional theory<sup>15,16</sup> (DFT) using the independent-particle approximation<sup>17</sup> (IPA) in order to investigate if cumulenes and polyynes can be distinguished by means of their optical spectra. The calculations have been carried out using the ABINIT<sup>18</sup> code. In order to support our findings, we have compared them with results within the Random-Phase approximation (RPA) including local-field (LF) effects performed using the YAMBO code.<sup>19</sup> We have derived our conclusions in two independent ways: on one hand side we have compared the low- and medium-energy spectral structure based on the DFT-IPA for our prototypes; on the other hand side we have drawn conclusion based on general spectral features which are obtained in both, the DFT-IPA and the RPA-LF results.

Polyynes prototypes are simulated using short (seven or eight C) carbon chains saturating the ends with one H atom at each side, while cumulene prototypes are simulated with two H atoms terminating each side; the latter case is also studied for different orientations of the planes to which the terminating  $\text{CH}_2$  belong, and the differences in the spectra are reported. The terminating groups contribution has been singled out by applying the so-called real-space cutoff technique,<sup>20,21,22</sup> which was originally developed for surfaces and which has been adapted here for molecules. Using this technique, the influence of the H termination of the carbon chains on the optical spectra has been determined.

This article is organized as follows: first, we introduce shortly the methodological background on which our calculations are based as well as the computational details (Sect. II). Then we inspect the groundstate properties of  $\text{C}_7\text{H}_n$  and  $\text{C}_8\text{H}_n$  chains ( $n = 2, 4$ ) with various lengths and H arrangements, where we investigate especially their bonding character and their magnetization (Sect. III). The bonding character and the spin polarization are reflected in their electronic properties (Sect. IV) on which the final results, the absorption spectra, are based (Sect. V). In the latter section, we discuss the spectral structure obtained within DFT-IPA by performing a detailed peak analysis as well as inspecting more gen-

eral spectral features. Besides, the influence of LF to the DFT-IPA is discussed. Finally, we summarize and draw our conclusions.

## II. THEORETICAL BACKGROUND AND COMPUTATIONAL DETAILS

In this section, the groundstate theory and the computational details are summarized as well as the basics for the calculation of optical spectra.

### A. Groundstate

Our investigation starts from *ab initio* total energy calculations using the ABINIT<sup>18,23</sup> code, which employs the density-functional theory scheme<sup>15</sup> (DFT) within the local-density approximation<sup>24,25</sup> (LDA). The eigenfunctions used to solve self consistently the Kohn-Sham equations<sup>16</sup> are expanded in plane waves and, for the ionic cores, we have chosen norm-conserving pseudopotentials in the Troullier-Martins style.<sup>26</sup> ABINIT is designed for a periodic-cell approach. The molecule is placed in a supercell and surrounded by vacuum to prevent the coupling to its periodic images. Due to the 0-dimensionality of the system only the  $\Gamma$  point is necessary to sample the reciprocal space. Therefore, the convergence of the groundstate depends on the kinetic-energy cutoff which determines the number of plane waves in the expansion and on the size of the supercell.

For an accurate groundstate, convergence requires a kinetic-energy cutoff of 20 Ha and a tetragonal supercell with lengths  $a = b = 25 a_B$  and  $c = 40 a_B$ . The carbon chain is oriented along the  $z$  direction ( $c$  axis). This choice of the convergence parameters yields total energy differences less than  $10^{-4}$  Ha. The carbynes have been relaxed till the remaining forces are less than  $5 \cdot 10^{-5}$  Ha/ $a_B$ . For details, see Ref. 27.

YAMBO<sup>19,28</sup> works directly on the ABINIT groundstate results and no additional groundstate calculations are necessary.

### B. Optical properties

The calculation of optical properties, in particular the photo-absorption cross section  $\sigma(\omega)$  as a function of the energy  $\omega$  is directly connected with the calculation of the polarizability function  $\alpha$ , since<sup>29</sup>

$$\sigma(\omega) = \frac{\omega}{c_0} \text{Im}[4\pi\bar{\alpha}(\omega)] \quad (1)$$

holds. Herein,  $\text{Im}[\bar{\alpha}(\omega)]$  is the imaginary part of the average (over the  $x$ ,  $y$ , and  $z$ ) polarizability function and  $c_0$  is the velocity of light. Thus it is sufficient to determine  $\text{Im}4\pi\bar{\alpha}(\omega)$ .

In a first step,  $\text{Im}[4\pi\bar{\alpha}(\omega)]$  has been calculated in the independent particle approach (IPA).<sup>17</sup> The probability  $P_{v\mathbf{k},c\mathbf{k}}$  of the transitions between valence ( $v$ ) and empty ( $c$ ) states with electronic eigenenergies  $E_{v\mathbf{k}}$  and  $E_{c\mathbf{k}}$  at a given  $\mathbf{k}$  point in the reciprocal space can be calculated as the matrix elements of the velocity operator. With these probabilities,  $\text{Im}[4\pi\alpha_\nu(\omega)]$  ( $\nu = x, y, z$ ) can be written as<sup>30</sup>

$$\text{Im}[4\pi\alpha_\nu(\omega)] = \frac{8\pi^2 e^2}{m^2 \omega^2} \sum_{\mathbf{k}} \sum_{v,c} |P_{v\mathbf{k},c\mathbf{k}}^\nu|^2 \times \delta(\Delta E - \hbar\omega) \quad , \quad (2)$$

where  $\Delta E = E_{c\mathbf{k}} - E_{v\mathbf{k}}$ , and  $m$  and  $e$  are the electronic mass and charge. In this approximation, only the matrix elements  $P_{v\mathbf{k},c\mathbf{k}}^\nu$  and the electronic eigenenergies are required. For molecules, the sum over  $\mathbf{k}$  can be reduced to the use of the  $\Gamma$  point only. Working within the DFT-IPA, local-field, self-energy, and excitonic effects are neglected.

In order to determine the influence of hydrogen termination of the chains, we have employed the real-space cutoff technique (see, e.g., Hogan *et al.*<sup>20</sup>) to the DFT-IPA spectra. With this technique the contribution of a selected region of the simulation cell can be filtered out by including a boxcar function in the calculation of the matrix elements. This function is equal to one in the desired region and zero elsewhere. We have implemented the matrix elements with and without real-space cutoff to the ABINIT<sup>18</sup> code and we have tested the implementation successfully.<sup>31</sup>

Beside the DFT-IPA, we have employed more elaborated methods in the framework of the TDDFT in the linear response formalism.<sup>32</sup> In brief, this approach requires the solution of the Dyson equation for the density response function. Here, also the standard Random-Phase approximation (RPA) with the inclusion of local-field (LF) effects is accessible. In order to obtain the polarizability function for interacting particles (which is directly related to the response function) one has to invert the Dyson equation. Usually, for periodic cell systems this is done in reciprocal space which can be quite cumbersome for supercell systems. Therefore, an alternative method is provided by the Casida approach,<sup>33,34,35,36,37</sup> which moves the task to the eigenvalue problem

$$\begin{pmatrix} A & B \\ B & A \end{pmatrix} = \omega \begin{pmatrix} 1 & 0 \\ 0 & -1 \end{pmatrix} \begin{pmatrix} x \\ y \end{pmatrix} \quad (3)$$

with  $A = \Delta E + U_0 + f_{xc}$  and  $B = U_0 + f_{xc}$ , where  $f_{xc}$  is the exchange-correlation kernel and  $U_0$  is the Coulomb interaction term. For details see, e.g., Refs 36 and 32. Eq. (3) is implemented in YAMBO<sup>19,28</sup> and allows the utilization of various approximations. Setting  $B = 0$  yields the Tamm-Dancoff approximation (TDA) whereas choosing  $f_{xc} = 0$  the standard RPA-LF.

We have performed calculations using YAMBO<sup>19,28</sup> employing the RPA-LF using both, the Dyson equation

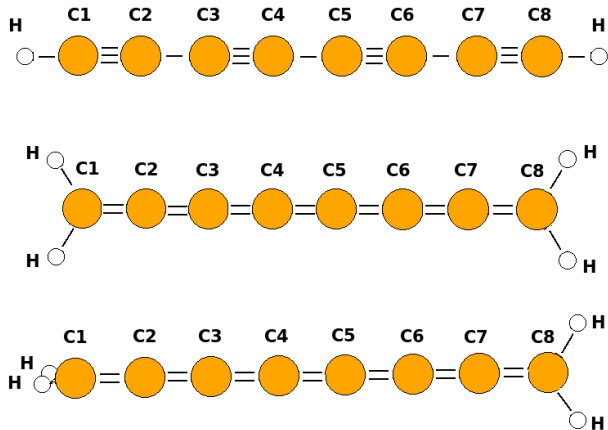


FIG. 1: (color online) Sketch of the carbynes  $C_8H_2$  (upper panel),  $C_8H_4$  in the  $D_{2h}$  (middle panel) and in the  $D_{2d}$  configuration (lower panel). Note the different bonding type of the molecules.

solution as well as the Casida approach.

### III. GROUNDSTATE PROPERTIES

In this study we consider the carbynes  $C_8H_2$  and  $C_8H_4$  as representatives for even atomic polyynes and cumulenes ( $C_8$  chains). In the latter case, the terminating hydrogens can have different orientations yielding the  $D_{2h}$  and  $D_{2d}$  symmetry. The  $D_{2h}$  has a planar configuration (all H and the carbon chain itself are in one plane) while for the  $D_{2h}$  one pair of H atoms is placed in a plane perpendicular to the one containing the other pair of H atoms, see Fig. 1. The same configurations are also studied for chains containing seven carbon atoms ( $C_7$  chains) as odd atomic prototypes. Besides, also longer polyynes with an even number of carbon atoms are inspected. Here we will discuss the groundstate properties in terms of bond length and magnetization.

#### A. Bond length

The relaxation of  $C_8H_4$  results in nearly equal C-C distances of 1.27–1.28 Å due to the double-bond character of all internal C-C bonds whereas for  $C_8H_2$  the single and triple bonds result in bond length of 1.33 and 1.23 Å, respectively (see Fig. 2), as expected from the literature. The distances C1-C2 and C7-C8 are slightly different due to the presence of the terminating H atoms. As one can see in Fig. 2, the configuration ( $D_{2h}$  or  $D_{2d}$ ) of  $C_8H_4$  does not influence the bond length significantly. Since the bond length of  $C_8H_4$  are equal, no change is expected for longer chains. Extending  $C_8H_2$  to  $C_{12}H_2$  and  $C_{16}H_2$ , one observes that the length of the triple bonds does not

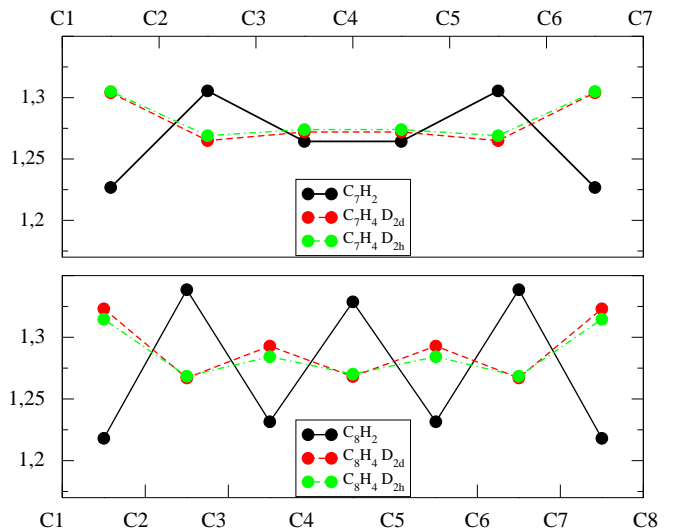


FIG. 2: (color online) Equilibrium bond lengths of  $C_7$  chains (upper panel) and  $C_8$  ones (lower panel).

change whereas the average length of the single bonds is slightly reduced to values around 1.31 Å.

Inspecting  $C_7H_4$  one obtains bond lengths very similar to the case of  $C_8H_4$  due to the double-bond character of the C-C bindings. The situation is completely different for  $C_7H_2$  due to the odd number of C atoms. In  $C_8H_2$  the C1-C2 and C7-C8 bonds at the end of the chain are both triple bonds and the alternation of single and triple bonds continues for the whole chain due to the even number of C atoms. For  $C_7H_2$ , the C-C bonds at the end of the chain are triple bonds which is reflected in the bond length of 1.23 Å similar to the corresponding bond length of  $C_8H_2$ . The neighboring bonds have a length of 1.31 Å which is between the length of the single and the double bonds of  $C_8H_2$ . The chain “tries” to obtain alternating bond length. In the middle of the chain, the alternation from both ends gets in conflict and results in bonds with length of 1.26 Å.

#### B. Analysis of the magnetization

Analyzing the groundstate properties we obtained the expected result, that  $C_8H_4$  in the  $D_{2d}$  configuration is magnetic, whereas  $C_8H_4$   $D_{2h}$  and  $C_8H_2$  are not. Since the  $D_{2d}$  differs only by the angle between the planes in which the H atoms are placed, we have investigated how the variation of angle between the planes containing the  $CH_2$  terminations affects the magnetization of the cumulenes, varying the angle from  $0^\circ$  ( $D_{2h}$ ) to  $90^\circ$  ( $D_{2d}$ ). For this reason, we have performed total-energy calculations forcing the Kohn-Sham orbitals to be occupied each with two electrons (spin up and spin down) like in the non-magnetic case of  $D_{2h}$  and on the other hand side, we imposed the spin configuration of the  $D_{2d}$  cumulene (magnetic). With these two setups, we have calculated

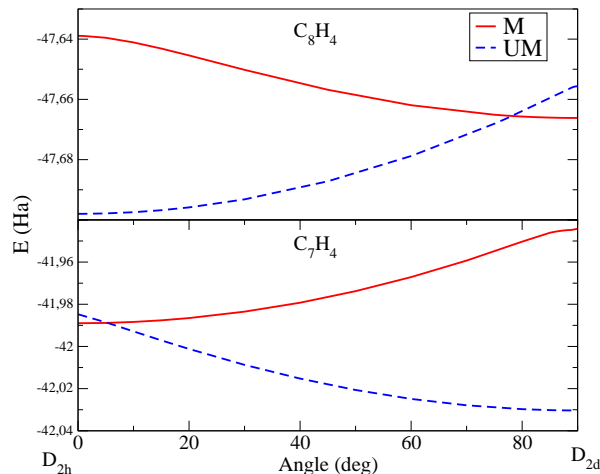


FIG. 3: (color online) Groundstate energy of  $C_8H_4$  (upper panel) and  $C_7H_4$  (lower panel) as a function of the relative angle between the H-H terminations. The solid line marks the magnetic (M) and the dashed line the non-magnetic (UM) configuration.

the total energy as a function of the rotation angle. The result for the  $C_8$  chains is presented in Fig. 3 (upper panel). Note that in the case of the  $D_{2h}$  configuration the absence of spin polarization is energetically preferred by 59 mHa, whereas for  $D_{2d}$  the spin-polarized setup is more stable than the spin-unpolarized one by 11 mHa. Turning the H terminations, the system prefers to remain in the unpolarized configuration until an angle of  $78^\circ$ . After this angle the magnetic configuration becomes energetically advantageous, as we found for  $C_8H_4$  in the  $D_{2d}$  symmetry. These findings are in agreement with the results of Ravagnan et al.<sup>6</sup> performed with a different numerical implementation of the DFT equations.

Interestingly, for the  $C_7$  chains the situation is opposite to the  $C_8$  ones. Here, the  $C_7H_2$  and  $C_7H_4$  with  $D_{2h}$  symmetry are magnetic, whereas the  $C_7H_4$  in the  $D_{2d}$  configuration is non-magnetic. Performing an analysis similar to the  $C_8H_4$  case, one finds that the  $D_{2h}$  and the configurations until an angle of  $5^\circ$  are magnetic, while the configurations for larger angles and the  $D_{2d}$  are non-magnetic as shown in Fig. 3 (lower panel). Here, the energy difference between the magnetic and the non-magnetic configuration for  $D_{2h}$  is 4 mHa while it is 86 mHa for  $D_{2d}$ .

#### IV. ELECTRONIC PROPERTIES

Optical transitions are excitations of electrons from a occupied state to an empty one in case of absorption. This is the basic assumption for DFT-IPA calculations. Furthermore, optical spectra can be interpreted inspecting the electronic states with respect to their (relative) energies and the charge density corresponding to these states. Thus, it is useful to inspect the electronic prop-

erties of the carbynes investigated here in detail.

The calculated electronic eigenenergies for our carbyne prototypes are schematically shown in Fig. 4. Since in the calculation of DFT-IPA spectra only energy differences are considered, we have shifted the energy range in such a way that the highest occupied molecular orbital (HOMO) is at 0 eV. In case of spin polarization we have chosen the HOMO of the major spin. The states close to the energy gap between the HOMO and the lowest unoccupied molecular orbital (LUMO) are energetically well distinguishable. Thus, one expects a clear structure of non-overlapping peaks in the low-energy range of the spectra.

The electronic states of  $C_8H_2$  close to the gap are double degenerate due to the cylindrical symmetry of the chain. Because of this, the coupled  $\pi_x$  and  $\pi_y$  single orbitals are at the same energy. The triple and single bonds are clearly distinguishable in charge density of the HOMO state (see Fig. 5). The linear  $sp$  bonds are present at lower energies, since they are more localized and feel more the attraction of the positive ions. LUMO states, instead, are placed around the odd bonds. There is a strong overlap between HOMO and LUMO around the carbons, in particular if we consider C1 and C8. Because of this, one expects that a significant contribution to the optical spectrum can be attributed to electronic transitions in the spatial region of the last carbon atoms next to the H terminations.

For  $C_8H_4$  in the  $D_{2h}$  configuration the cylindrical symmetry is broken, so the electronic states are no more degenerate, and there is an alternation of  $x$  and  $y$  polarized states. The HOMO of  $C_8H_2$  splits into  $C_8H_4$  ( $D_{2h}$ ) HOMO-1 and LUMO, since the corresponding charge density is very similar. An analogous situation occur for the LUMO of  $C_8H_2$  (see Fig. 5), which splits into HOMO and LUMO+1. The overlap between HOMO and LUMO is zero, since they are orthogonally polarized, so we do not expect an absorption peak for a transition involving these states. On the contrary, HOMO and LUMO+1 show a charge-density distribution on the same plane. The same applies to HOMO-1 and LUMO. For the latter states, we see in Fig. 5 an important overlap around the termination, because these two states are polarized orthogonally to the hydrogen plane. The contribution of this region should be corrected by the real-space cutoff in order to eliminate the H contribution to the spectra.

A mixed situation arises for  $C_8H_4$  in the  $D_{2d}$  symmetry. Here only the bands between HOMO-4 and LUMO are double degenerate for spin up and the bands between HOMO-3 and LUMO+1 for spin down. Majority and minority electron densities have a very similar shape, therefore only one component is shown in the Fig. 5. The  $\pi$ -derived HOMO-1 can be understood as a result of the merging of the HOMO-1 and HOMO of the planar conformer.

Regarding the degeneracies and the splitting of eigenstates, the  $C_8$  and the  $C_7$  chains are very similar. However, the different bonding character of  $C_7H_2$  is reflected

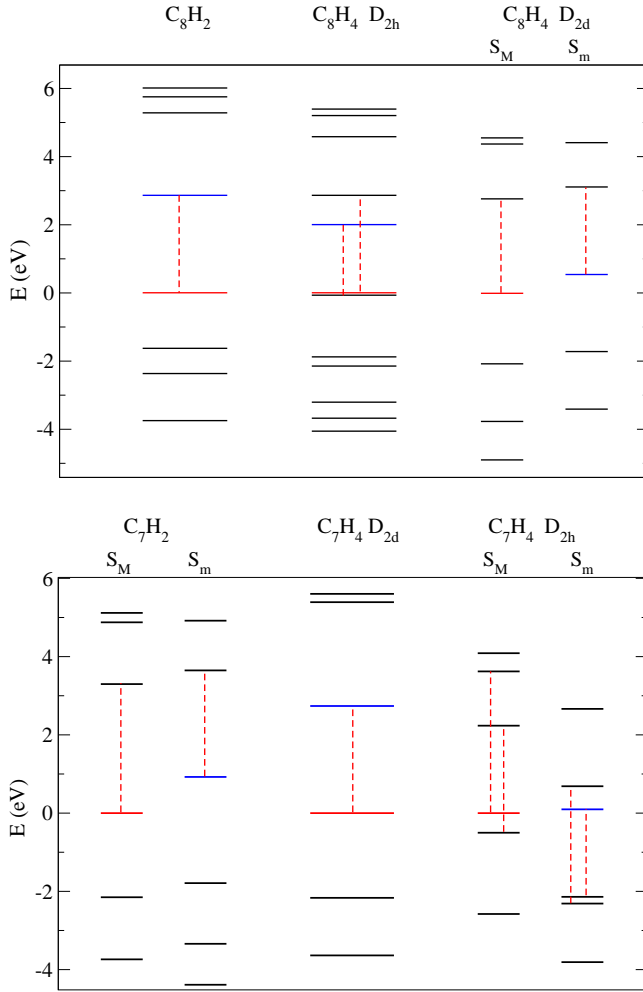


FIG. 4: (color online) Schematic presentation of the relative positions of the DFT eigenenergies for the considered  $C_8$  chains (upper panel) and the  $C_7$  ones (lower panel). For magnetic chains, the eigenenergies for the major (M) and minor (m) spin is broken down. The energy scale is shifted to HOMO=0 eV (of the major spin for magnetic configurations). The main optical transitions within DFT-IPA are marked with dashed lines.

in the charge-density distribution of the HOMO and the HOMO-1. While for  $C_8H_2$  the charge density is placed around the triple bonds for the HOMO, for the  $C_7H_2$  it is localized at C atoms. Especially in the HOMO-1, the difference due to the even/odd number of C atoms can be seen: for  $C_7H_2$  the corresponding charge density covering the three C atoms localized in the center of the molecule.

Looking forward to the calculation of the optical spectra and the use of the real-space cutoff, the polyynes and the cumulenes should be treated differently. Cumulenes are chains of the style  $C_{n-2}(CH_2)_2$  and thus the termination of the chain contains not only H but also C. Because of this, the cut should be placed between the last two C atoms of the chain and cutting of a complete  $CH_2$  group. Inspecting the charge density for the states close to the

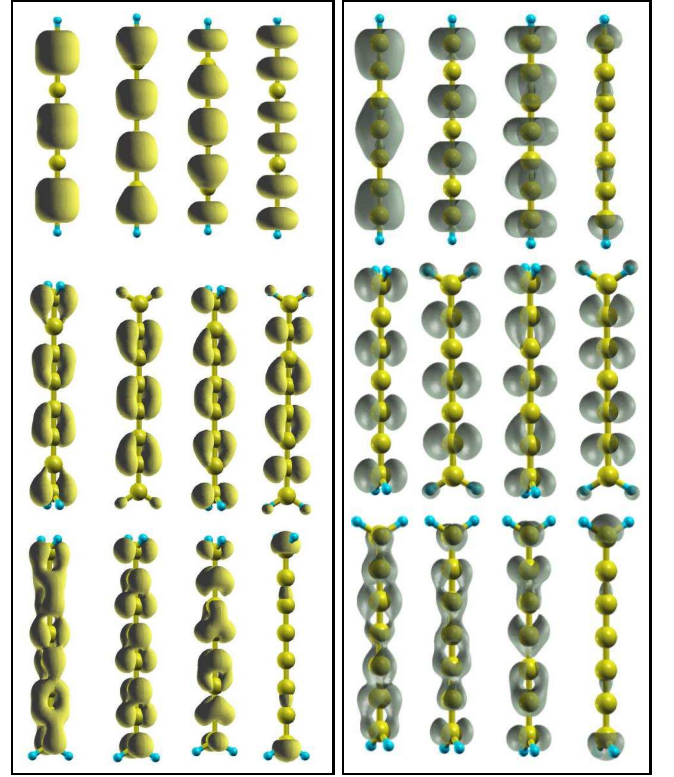


FIG. 5: (color online) Charge density for  $C_8$  chains (left panel) and  $C_7$  ones (right panel); for each panel, from the top to bottom, for the polyynes (upper panel), the  $D_{2h}$  cumulene (middle panel), and the  $D_{2d}$  one the HOMO-1, HOMO, LUMO, and LUMO+1 are presented from left to right.

gap, only a little amount of charge is cut in the middle and therefore, unphysical spectral features might be avoided. On the contrary, for the polyynes the termination consists only of H resulting in a cut between the C and H atom. As shown in Fig. 5, for states close to the HOMO-LUMO gap, nearly no charge density would be cut.

In general, the charge-density distribution is very regular leading the conclusion that a similar distribution will be found even for longer chains. The only chain where charge-density differences might be found is  $C_7H_2$  where the regimes showing alternating bonds and double bonds have different extents for longer chains.

## V. OPTICAL PROPERTIES

In this section we present our results for the optical spectra of our polyynes and cumulene prototypes. In a first step, we analyze the spectral structure of our DFT-IPA spectra where we compare the peak positions in the low- and medium-energy range (Sect. V A). Here, we have investigated also the contribution of the terminating H atoms to the spectra using the real-space cutoff technique (Sect. V B).



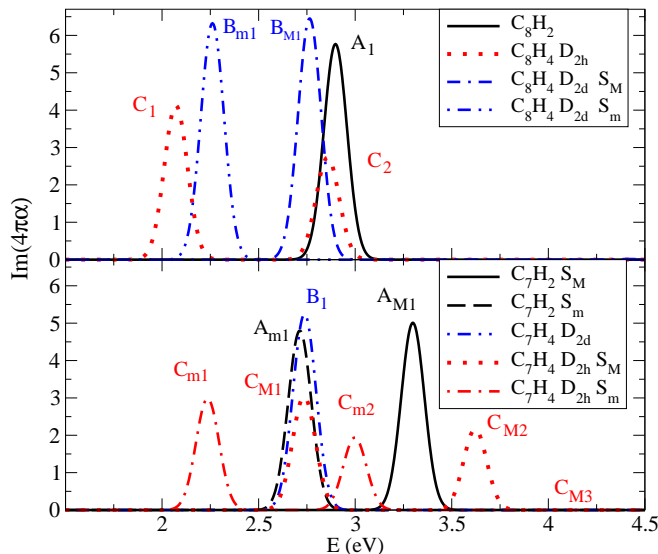


FIG. 6: (color online) Comparison of the imaginary part of the polarizability function as a function of the energy for the  $\text{C}_8$  chains (upper panel) and the  $\text{C}_7$  chains (lower panel).  $\text{S}_M$  correspond to major spin,  $\text{S}_m$  to minor spin spectra. The peaks are labeled with A for polyynes, B for  $\text{D}_{2d}$  cumulenes, and C for  $\text{D}_{2h}$  cumulenes. Here only the low-energy range is shown.

Since the DFT-IPA yields fast but not highly accurate results, an alternative scheme for distinguishing the considered six prototypical chains has been developed based on general features observed in the optical spectra (Sect. VC). In order to confirm the basic ingredients for this scheme, we have performed RPA-LF calculations for the non-magnetic systems  $\text{C}_8\text{H}_2$ ,  $\text{C}_8\text{H}_4$  ( $\text{D}_{2h}$ ), and  $\text{C}_7\text{H}_4$  ( $\text{D}_{2d}$ ) (Sect. VI).

### A. Spectra within DFT-IPA

For the calculation of the imaginary part of the dielectric function it was possible to reduce the kinetic-energy cutoff to 18 Ha without losing significant accuracy (for detail with respect to this parameter, see Ref. 31). This leads to a faster but equally accurate calculation. Another important parameter is the number of empty states to be considered (see Eq. 2). For molecules the continuum states should be excluded, since an excitation of the molecule to these states corresponds to ionization. Continuum states are extended in space and thus, the eigenenergies corresponding to these states vary with the size of the supercell. An inspection of the energy of many states as a function of the size of the supercell yields the result that the energy of the states up to LUMO+7 is not influenced significantly by the size of the simulation box while the others are. Thus, we have considered in our calculation 8 empty states. Beside the parameters mentioned here, all other parameters are kept the same as for the groundstate calculations.

The calculated spectra of the imaginary part of the polarizability function as a function of the energy for  $\text{C}_8\text{H}_2$ ,  $\text{C}_8\text{H}_4$  ( $\text{D}_{2h}$  and  $\text{D}_{2d}$ ),  $\text{C}_7\text{H}_2$ , and  $\text{C}_7\text{H}_4$  ( $\text{D}_{2h}$  and  $\text{D}_{2d}$ ) are presented in Fig. 6 (low-energy range) and Fig. 7 (medium-energy range), where also the resolution in major and minor spin contributions is given for magnetic compounds.

Inspecting the low-energy range of the spectra of  $\text{C}_8\text{H}_2$  (Fig. 6), one notice immediately that the three considered prototypes are clearly distinguishable by their spectral structure:  $\text{C}_8\text{H}_2$  has only one strong peak (marked with  $\text{A}_1$  in the figure) at 2.90 eV which results from transitions between the HOMO and LUMO states. This transition involves electrons in the  $\pi_x$  and  $\pi_y$  molecular orbitals (see Fig. 5), which are degenerate due to cylindrical symmetry. Thus, the peak is polarized in  $z$  direction. For the non-magnetic  $\text{C}_8\text{H}_4 \text{D}_{2h}$  cumulene the main peak is split into two peaks, whose energies are 2.07 eV and 2.85 eV. Since the cylindrical symmetry is broken, both the HOMO and LUMO states of  $\text{C}_8\text{H}_2$  are split in two states for  $\text{C}_8\text{H}_4$  (see Fig. 4). Here the HOMO→LUMO transition is forbidden because the respective wave functions lie in the  $x$ - $z$  and  $y$ - $z$  planes. The peaks are due to the transitions HOMO-1→LUMO (2.07 eV,  $\text{C}_1$ ) and HOMO→LUMO+1 (2.85 eV,  $\text{C}_2$ ). The  $\text{C}_8\text{H}_4 \text{D}_{2d}$  shows also a double-peak structure, however, one peak is due to a major-spin (2.76 eV,  $\text{B}_{M1}$ ) and the other due to a minor-spin (2.26 eV,  $\text{B}_{m1}$ ) transition. Both transitions are HOMO-LUMO ones. From the low-energy range of the DFT-IPA spectra one can conclude that the  $\text{C}_8$  chains can be distinguished in optical spectra, since the polyyne prototype shows only one main peak whereas the cumulenes show a double-peak structure. The two cumulenes can be distinguished in symmetry due to the fact that one is magnetic and the other not.

Since the  $\text{C}_8\text{H}_2$  polyyne might have not exactly the cylindrical symmetry in the experiment, we have also calculated the groundstate and the spectrum of a non-linear configuration of  $\text{C}_8\text{H}_2$  where we altered the carbon positions in order to create a zig-zag configuration shifting the carbons of the molecule (which is oriented along the  $z$  axis) in the  $x$  or  $y$  direction by a displacement of about the 5 % of bond lengths. In this way we have broken the cylindrical symmetry. Because of this, the main peak  $\text{A}_1$  is split in two close peaks at 2.85 eV and 2.80 eV. For peaks at higher energy we have found that the higher is the energy of the peak, the higher is its energy splitting. Nevertheless, this split is much less than the ones of the cumulenes ( $\text{C}_1$ ,  $\text{C}_2$  and  $\text{B}_{M1}$ ,  $\text{B}_{m1}$ , respectively) and thus, the conclusion from above remains valid also in this case.

Inspecting the spectra of the  $\text{C}_7$  chains, one observes a clear spectral structure as in the  $\text{C}_8$  case.  $\text{C}_7\text{H}_2$  is magnetic and the HOMO-LUMO transition splits into two peaks at 3.30 eV ( $\text{A}_{M1}$ , major spin) and at 2.71 eV ( $\text{A}_{m1}$ , minor spin). Similarly, the non-magnetic  $\text{C}_7\text{H}_4$  ( $\text{D}_{2d}$ ) shows only one peak at 2.74 eV ( $\text{B}_1$ ) due to the HOMO-LUMO transition. This peak appeared split

for the magnetic  $C_8H_4 D_{2d}$  cumulene. The magnetic  $C_7H_4 D_{2h}$  shows four transitions: for the major spin we have the HOMO-1→LUMO (2.74 eV,  $C_{M1}$ ) and the HOMO→LUMO+1 (3.62 eV,  $C_{M2}$ ) one and for the minor spin a HOMO→LUMO (2.23 eV,  $C_{m1}$ ) and a HOMO-1→LUMO+1 (2.99 eV,  $C_{m1}$ ) one. As for the  $C_8$  case, comparing the  $C_7$  chains one can conclude that the three prototypes can be distinguished since we have four peaks for  $C_7H_4 D_{2h}$ , two peaks for  $C_7H_2$ , and one peak for  $C_7H_4 (D_{2d})$ .

Comparing the DFT-IPA spectra for the  $C_7$  and the  $C_8$  chains, from the spectral structure all types of chains could be identified in experiments if their magnetization is known. The four-peak feature of  $C_7H_4 D_{2h}$  is unique. We have two magnetic double-peak features ( $C_8H_4 D_{2d}$  and  $C_7H_2$ ) which are distinguishable due to the transition energy. We have one unique non-magnetic double peak for  $C_8H_4 D_{2h}$ . The only chains which cannot be distinguished unambiguously from the low-energy range of the DFT-IPA spectra are  $C_8H_2$  and  $C_7H_4 D_{2d}$  which are both non-magnetic and show only a single peak which differs in energy only about 0.1 eV. Note, that in the low-energy range all peaks shown in Fig. 6 are  $z$  polarized.

Unfortunately, DFT-IPA spectra usually can give only a rough idea of what might be seen in the experiment. Comparing spectra performed with TDDFT methods or those which are based on solutions of the Bethe-Salpeter equation (for an overview of methods and results see, e.g., Ref. 29), one observes not only a shift of the peaks but also a shift of the oscillator strength to higher energies which is not uniform. Nevertheless, the low-energy transitions will contribute also to the corresponding peaks at TDDFT level, though, possibly at less extent. Regarding the shift of peak positions and oscillator strength to higher energies, the medium and high-energy range can be enhanced. Therefore, we inspect the medium-energy range of our DFT-IPA spectra, too.

For the medium energy range up to 7 eV (see Fig. 7) a clear spectral structure is absent as well as for the high-energy range (not shown here). In this range, the DFT-IPA spectra shows only a low intensity, which is of about 0.5%–2.5% of the intensity in the low-energy range. The spectral features involve transitions from states down to HOMO-5 to states up to LUMO+5. Inspecting the transitions, no general trends have been found. Considering the polarization of the transitions, most of the peaks are  $z$  polarized. The remaining peaks have an  $x$  and/or  $y$  component only. Considering the magnetic compounds, one sees that some of the peaks for major and minor spin coincide in energy. For  $C_8H_4 D_{2d}$  we have two of these peaks,  $B_{M2/m2}$  and  $B_{m4}/B_{M4}$ . For  $C_7H_4 D_{2h}$  it is only one, namely  $C_{M5/m5}$  and for  $C_7H_2$  it is  $A_{M3/m4}$ .

## B. Spectra using the real-space cutoff

The DFT-IPA technique gives us the possibility to determine the contribution of the terminating H atoms to

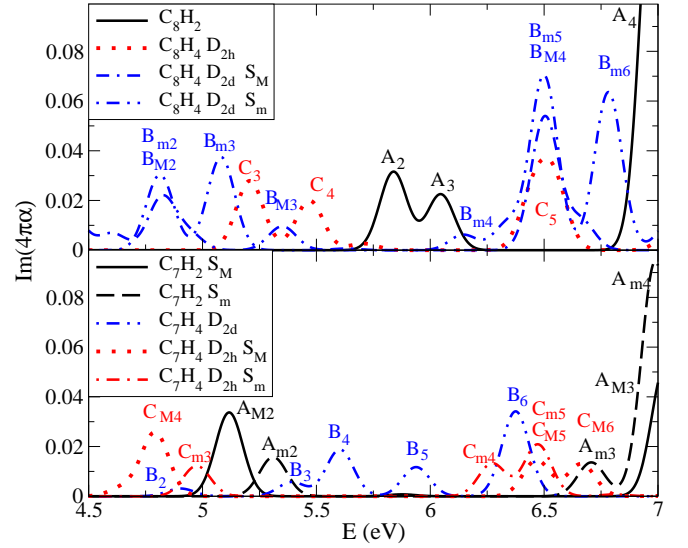


FIG. 7: (color online) Same as in Fig 6 for the medium-high energy range.

the spectra by employing the real-space cutoff introduced by various groups, see e.g., Refs. 20,21,22. As discussed in Sect. IV, the best choice of eliminating the H termination would be to cut the H atoms only for polyynes and the terminating  $CH_2$  group for cumulenes. However, the resulting chains would not be comparable in intensity due to the different number of remaining C atoms. Thus, we have decided to eliminate the terminating H atoms together with the neighboring C atom (resulting in the  $CH_2$  group for cumulenes and a  $CH$  group for polyynes) by applying the real-space cutoff for the polyynes and cumulenes in the same range.

Inspecting the low-energy range, we have found a lowering of around 25% of the main peaks for the  $C_8$  chains applying the real-space cutoff. This can be explained by the fact that we have cut also one C atom at each end and thus, the contribution of the H atoms is very small. We can also conclude, that the intensity of the peaks is determined by the number of C atoms in the chain which is confirmed by comparing the intensities of the  $C_8$  and the  $C_7$  chains in Fig. 6. Thus, one expects for longer chains not only spectra containing more peaks (since there are more non-continuum states to consider) but also with a larger intensity.

## C. Conclusions from general considerations

Often DFT-IPA spectra are not able to predict a quantitative correct peak structure. Thus, we have analyzed our spectra also from a more general point of view in order to find an alternative way to draw conclusion. At higher energies mainly  $x$  and  $y$  polarized peaks are observed, whereas only few  $z$  polarized feature appear. Looking at the  $z$  polarized peaks only, we have found a

gap of at least 2 eV between the last  $z$  polarized peaks and the following high-energy  $z$  polarized feature. This inset of the gap is placed at around 8-10 eV and depends on the kind of the chain. Similarly, in the low- and medium-energy range up to about 9 eV only few peaks with  $x$  and/or  $y$  component are found. This brings us to the conclusion that the spectra can be divided in energy range: in the low and medium energy range the  $z$  component plays a major role whereas in the high-energy range the spectra is determined by  $x$  and  $y$  polarized peaks. This observation is useful for further considerations, since it allows the counting of  $z$  polarized peaks in the low-energy range till the gap inset.

Inspecting other general features of the chains like symmetry and magnetization, we are able to draw conclusion without detailed peak analysis.

In a first step, the six chains can be divided into two groups, the magnetic chains  $C_8H_4$  ( $D_{2d}$ ),  $C_7H_2$ , and  $C_7H_4$  ( $D_{2h}$ ) and the non-magnetic chains  $C_8H_2$ ,  $C_8H_4$  ( $D_{2h}$ ), and  $C_7H_4$  ( $D_{2d}$ ), which can be discriminated by the presence of a magnetic moment.

The second step is guided by symmetry considerations: in each group there is only one chain which has no  $xy$  symmetry: the magnetic  $C_8H_4$  ( $D_{2h}$ ) and the non-magnetic  $C_7H_4$  ( $D_{2h}$ ) where the  $x$  and  $y$  components of the spectra differ. For these chains one expects spectral changes (in the high-energy regime where  $x$  and  $y$  polarized features appear) for  $x$  and  $y$  polarized light.

For the last step we exploit the fact that the spectra can be divided into two zones: the range up to 8-10 eV where the spectra shows mainly  $z$  polarization and the range beyond 8-10 eV, where the spectra has mainly  $x$  and  $y$  polarization. This range is separated by a gap of at least 2 eV from the next small  $z$  polarized peak. Since for the polyne chains some states close to the HOMO-LUMO gap are degenerate, one expects less peaks for  $C_7H_2$  and  $C_8H_2$  than for  $C_8H_4$  ( $D_{2d}$ ) and  $C_7H_4$  ( $D_{2d}$ ) in the magnetic and non-magnetic case, respectively. Since the spectra in this range show mainly  $z$  polarized peaks, we are able to count these peaks till the inset of the gap: in the energy range up to about 10 eV we have three peaks for  $C_8H_2$ , 6 peaks for  $C_8H_4$  ( $D_{2h}$ ), 5 peaks for  $C_8H_4$  ( $D_{2d}$   $S_M$ ), and 7 peaks for  $C_8H_4$  ( $D_{2d}$   $S_m$ ). Similarly, there are 2 peaks for  $C_7H_2$  ( $S_M$ ), 3 peaks for  $C_7H_2$  ( $S_m$ ), 4 peaks for  $C_7H_4$  ( $D_{2d}$ ), 4 peaks for  $C_7H_4$  ( $D_{2h}$   $S_M$ ), and 6 peaks for  $C_7H_4$  ( $D_{2h}$   $S_m$ ). For the comparison of  $C_7H_2$  with  $C_8H_4$  ( $D_{2d}$ ) (both magnetic) this means that we have  $2/3$  ( $S_M/S_m$ ) against  $5/7$  ( $S_M/S_m$ ) or in total 6 against 8, while for  $C_8H_2$  and  $C_7H_4$  ( $D_{2d}$ ) there are 3 against 4 peaks.

With these simple considerations we have shown, that the 6 chains can be distinguished by optical spectra without the necessity of a detailed peak analysis.

## VI. SPECTRA USING RPA-LF

In order to inspect spectral changes using more advanced methods, we have performed calculations using the RPA-LF. The main scope here is to confirm the validity of the general conclusions, in particular, the existence of the gap which is used to design a criterium for the peak counting and the number of peaks in the low- and medium energy range. For this reason, it was sufficient to do calculations not at full convergence, which is difficult to achieve. For this test we have performed calculations for the non-magnetic chains  $C_8H_2$ ,  $C_8H_4$  ( $D_{2h}$ ), and  $C_7H_4$  ( $D_{2d}$ ) only.

The results show mainly the expected shift of peak positions and oscillator strength to higher energies. In detail, we have found a strong shift to higher energies of the peaks shown in Fig. 6, which now appear at energies around 5-6 eV, and an enhancement of the peaks with  $z$  polarization shown in Fig. 7. The shift is not uniform for the low-energy peaks. For example we have found for  $C_8H_4$  only one strong peak followed by three small peaks whereas at DFT-IPA there are two strong peaks. Instead for  $C_7H_4$  a double-peak structure with strong intensity appear followed by a less intense double-peak structure. It is possible that the first strong-intensity double feature merge to one peak at higher convergence. For  $C_8H_2$  a strong peak remained followed by two small ones. Nevertheless, the three non-magnetic chains still show a different spectral structure and are therefore distinguishable by means of optical measurements.

Regarding the general conclusions of Sect. VC, we have found that for the  $z$  polarized peaks the oscillator strength are shifted from the high-energy peaks (above the gap) to the low-energy ones, while the  $x$  and  $y$  component remained nearly unchanged in intensity. Since the high-energy  $z$  polarized peaks have a very small intensity, a considerable spectral structure has been found only up to 8/9 eV followed by a gap of 2 eV. Thus, a counting of the peaks is also possible here. In particular, we have found 3 peaks for  $C_8H_2$  compared to 3 peaks DFT-IPA, four peaks for  $C_8H_4$  ( $D_{2h}$ ) compared to 6 peaks DFT-IPA, and 5 peaks (2 strong double peaks followed by a tiny one) for  $C_7H_4$  ( $D_{2d}$ ) compared to 4 peaks DFT-IPA. Also here,  $C_8H_2$  and  $C_7H_4$  ( $D_{2d}$ ) are distinguishable by the number of  $z$  polarized peaks.

In summary, employing the RPA-LF we find similar spectral features as in the DFT-IPA which have been used for our general conclusions.

## VII. SUMMARY AND CONCLUSION

We have performed an *ab initio* investigation of carbyne prototypes inspecting their groundstate and optical properties in detail using DFT based methods. We have considered seven- and eight-atomic chains saturated with one H (polyne prototype) and two H (cumulene prototype) at each end, respectively. Polynes and cumulenes



have a different bonding character. While the cumulenes show always double bonds, the polyynes have an alternating triple-single bond character. In case of odd-atomic chains, we have observed that this alternation results in the accidental building bonds similar to double bonds in the middle of the chain. Regarding the cumulenes, there are two possible symmetry configuration, namely  $D_{2h}$  and a  $D_{2d}$ , corresponding to placing the saturating H atoms all in one plane or placing them in planes perpendicular to each other. Depending on the symmetry, the  $C_8H_4$   $D_{2d}$  is magnetic and  $C_8H_4$   $D_{2h}$  is not. For  $C_7H_4$  the situation is reversed: here the  $D_{2h}$  chain is magnetic whereas  $C_7H_4$  is non-magnetic. Rotating the H atoms, we have observed that the angle for which the cumulene becomes magnetic is different for even- and odd-atomic chains. Considering the optical spectra, we have found that the H terminations give only tiny contributions to the spectra. From the analysis of our DFT-IPA spectra we have seen that the six carbynes considered here are distinguishable by their optical spectra. However, due to well-known problems of the DFT-IPA a quantitative conclusion cannot be drawn unambiguously. Nevertheless, we have been able to draw a scheme to distinguish the chains unambiguously based on the general features of the calculated spectra (within DFT-IPA and RPA-LF), the spin polarization of the systems, and their symmetry. With this scheme, the carbynes  $C_8H_2$ ,  $C_8H_4$   $D_{2h}$ ,  $C_8H_4$   $D_{2d}$ ,  $C_7H_2$ ,  $C_7H_4$   $D_{2h}$ , and  $C_7H_4$   $D_{2d}$  can be dis-

tinguished. It might be possible to extend this scheme also for longer chains.

To apply our scheme, one needs the knowledge of the magnetization of the system and polarization resolved optical spectra are necessary. However, more accurate calculations might give quantitative spectra from which the chains can be distinguished by absorption spectra only without inspection of the magnetization of the chains and/or polarization resolution of the spectra. These calculations might be accelerated due to the fact, that the low-energy range of the spectra is mainly  $z$  polarized and thus a detailed inspection of the  $x$  and  $y$  component is not necessary. We hope that this study here will encourage further theoretical and experimental investigations of carbynes.

### Acknowledgment

The authors thank Giovanni Onida, Silvana Botti, and Davide Sangalli for fruitful discussions. This work was funded by the EU's 6th Framework Programme through the NANOQUANTA Network of Excellence (NMP-4-CT-2004-500198) and the EU's 7th Framework Programme through the e-I3 ETSF initiative (Grant agreement No. 211956).

- 
- \* Electronic address: katalin.gaal-nagy@physik.uni-r.de
- <sup>1</sup> T. Kawai, S. Okada, Y. Miyamoto, and A. Oshiyama, Phys. Rev. B **72**, 035428 (2005).
  - <sup>2</sup> P. Darancet, V. Olevano, and D. Mayou, Phys. Rev. Lett. **102**, 136803 (2009).
  - <sup>3</sup> J. Kong, N. R. Franklin, C. Zhou, M. G. Chapline, S. Peng, K. Cho, and H. Dai, Science **287**, 622 (2000).
  - <sup>4</sup> A. Lucotti, M. Tommasini, M. D. Zoppo, C. Castiglioni, G. Zerbi, F. Cataldo, C. Casari, A. L. Bassi, V. Russo, M. Bogana, et al., Chem. Phys. Lett. **417**, 78 (2006).
  - <sup>5</sup> X. Gu, R. Kaiser, and A. Mebel, Chem. Phys. Chem. **9**, 350 (2008).
  - <sup>6</sup> L. Ravagnan, N. Manini, E. Cinquanta, G. Onida, D. Sangalli, C. Motta, M. Devetta, A. Bordon, P. Piseri, and P. Milani, Phys. Rev. Lett. **102**, 245502 (2009).
  - <sup>7</sup> C. Jin, H. Lan, L. Peng, K. Suenaga, and S. Iijima, Phys. Rev. Lett. **102**, 205501 (2009).
  - <sup>8</sup> C. S. Casari, A. Li Bassi, L. Ravagnan, F. Siviero, C. Lenardi, P. Piseri, G. Bongiorno, C. E. Bottani, and P. Milani, Phys. Rev. B **69**, 075422 (2004).
  - <sup>9</sup> E. Magnano, C. Cepek, M. Sancrotti, F. Siviero, S. Vinati, C. Lenardi, P. Piseri, E. Barborini, and P. Milani, Phys. Rev. B **67**, 125414 (2003).
  - <sup>10</sup> L. Ravagnan, F. Siviero, C. Lenardi, P. Piseri, E. Barborini, P. Milani, C. S. Casari, A. L. Bassi, and C. E. Bottani, Phys. Rev. Lett. **89**, 285506 (2002).
  - <sup>11</sup> A. Scemama, P. Chaquin, M.-C. Gazeau, and Y. Bnilan, Chem. Phys. Lett. **361**, 520 (2002).
  - <sup>12</sup> S. Hino, Y. Okada, K. Iwasaki, M. Kijima, and H. Shirakawa, Chem. Phys. Lett. **372**, 59 (2003).
  - <sup>13</sup> M. Grutter, M. Wyss, J. Fulara, and J. Maier, J. Phys. Chem. A **102**, 9785 (1998).
  - <sup>14</sup> C. Ball, M. McCarthy, and P. Taddheus, J. Chem. Phys. **112**, 10149 (2000).
  - <sup>15</sup> P. Hohenberg and W. Kohn, Phys. Rev. **136 B**, 864 (1964).
  - <sup>16</sup> W. Kohn and L. J. Sham, Phys. Rev. **140 A**, 1133 (1965).
  - <sup>17</sup> H. Ehrenreich and M. H. Cohen, Phys. Rev. **115**, 786 (1959).
  - <sup>18</sup> <http://www.abinit.org>.
  - <sup>19</sup> <http://www.yambo-code.org>.
  - <sup>20</sup> C. Hogan, R. DelSole, and G. Onida, Phys. Rev. B **68**, 035405 (2003).
  - <sup>21</sup> C. Castillo, B. S. Mendoza, W. G. Schmidt, P. H. Hahn, and F. Bechstedt, Phys. Rev. B **68**, 041310(R) (2003).
  - <sup>22</sup> P. Monachesi, M. Palummo, R. DelSole, A. Grechnev, and O. Eriksson, Phys. Rev. B **68**, 035426 (2003).
  - <sup>23</sup> X. Gonze, G.-M. Riganese, M. Verstraete, J.-M. Beuken, Y. Pouillon, R. Caracas, F. Jollet, M. Torrent, G. Zerah, M. Mikami, et al., Z. Kristallogr. **220**, 558 (2005).
  - <sup>24</sup> D. M. Ceperley and B. J. Alder, Phys. Rev. Lett. **45**, 566 (1980).
  - <sup>25</sup> J. P. Perdew and A. Zunger, Phys. Rev. B **23**, 5048 (1981).
  - <sup>26</sup> N. Troullier and J. L. Martins, Phys. Rev. B **43**, 1993 (1991).
  - <sup>27</sup> C. Motta, Master's thesis, Università degli Studi di Milano (2007-2008).
  - <sup>28</sup> A. Marini, C. Hogan, M. Grüning, and D. Varsano, Comp.

- Phys. Commun. p. doi:10.1016/j.cpc.2009.02.003 (2009).
- <sup>29</sup> G. Onida, L. Reining, and A. Rubio, Rev. Mod. Phys. **74**, 601 (2002).
- <sup>30</sup> G. F. Bassani, in *Electronic states and optical transitions in solids* (Pergamon Press, Oxford, 1975), p. 149.
- <sup>31</sup> C. Motta, M. Cazzaniga, M. Giantomassi, K. Gaál-Nagy, G. Onida, and X. Gonze, Preprint (2009).
- <sup>32</sup> M. A. L. Marques and E. K. U. Gross, Ann. Rev. Phys. Chem. **55**, 427 (2004).
- <sup>33</sup> M. E. Casida, K. C. Casida, and D. R. Salahub, Int. Jour. Quant. Chem. **70**, 933 (1998).
- <sup>34</sup> M. E. Casida, C. Jamorski, K. C. Casida, and D. R. Salahub, Jour. Chem. Phys. **108**, 4439 (1998).
- <sup>35</sup> C. Jamorski, M. E. Casida, and D. R. Salahub, Jour. Chem. Phys. **104**, 5134 (1996).
- <sup>36</sup> M. E. Casida and T. A. Wesolowski, Int. Jour. Quant. Chem. **96**, 577 (2004).
- <sup>37</sup> I. Vasiliev, S. Ögut, and J. R. Chelikowsky, Phys. Rev. Lett. **82**, 1919 (1999).